ACS APPLIED MATERIALS & INTERFACES

Research Article

www.acsami.org

Improved Performance of Organic Light-Emitting Diodes Fabricated on Al-Doped ZnO Anodes Incorporating a Homogeneous Al-Doped ZnO Buffer Layer Grown by Atomic Layer Deposition

Yong-June Choi,[†,‡] Su Cheol Gong,[†,‡] Chang-Sun Park,[†] Hong-Sub Lee,[†] Ji Geun Jang,[§] Ho Jung Chang,[§] Geun Young Yeom,[⊥] and Hyung-Ho Park*[,†]

[†]Department of Materials Science and Engineering, Yonsei University, Seoul 120-749, Republic of Korea

[§]Department of Electronics Engineering, Dankook University, Cheonan-si, Chungcheongnam-do 330-714, Republic of Korea

[⊥]Department of Advanced Materials Science and Engineering and SKKU Advanced Institute of Nanotechnology, Sungkyunkwan University, Suwon, Kyunggi-do 440-746, Republic of Korea

ABSTRACT: In this work, we investigated the use of a homogeneous Al-doped zinc oxide (AZO) buffer layer to improve the performance of an organic light-emitting diode (OLED) device fabricated on an AZO anode. For this, 10-nm-thick AZO buffer layers with Al doping concentrations of 3.1, 4.1, and 5.1 at % were grown on 140-nm-thick AZO anode films containing 2.1 at % Al by atomic layer deposition. The electrical resistivity of the AZO anode with a homogeneous AZO buffer layer decreased with an increase in Al doping concentration up to 4.1 at %; however, the resistivity increased at higher doping concentrations in the AZO buffer layer. On the other hand, the work functions of the AZO anode with the AZO buffer layer containing various Al doping concentrations gradually increased with an increase in Al doping concentration from 3.1 to 5.1 at %. Therefore, the best film properties were obtained for an AZO anode with an AZO buffer layer containing 4.1 at % Al, and the work function value for this film was 4.64 eV. The highest luminance and current efficiency values were optimized to be 20290 cd/m^2 and 13.4 cd/A, respectively, with the OLED device composed of a DNTPD/TAPC/Bebq$_2$:10% doped RP-411/Bphen/LiF/Al structure on an AZO anode with an AZO buffer layer containing 4.1 at % Al.

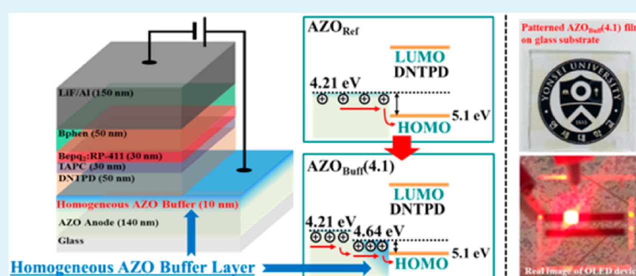

KEYWORDS: *Al-doped ZnO (AZO), transparent conducting oxide (TCO), organic light-emitting diodes (OLEDs), anode buffer layer, work function, atomic layer deposition (ALD)*

■ INTRODUCTION

Organic light-emitting diodes (OLEDs) have potential for use in next-generation displays and solid-state lighting because they are self-emitting, thin, lightweight, and have low power consumption, which makes them suitable for flexible display applications.[1] Currently, OLEDs are already in use for small flat panel displays such as those in smart phones, digital cameras, and most mobile displays. Therefore, much research has focused on improving the luminance and current efficiency of OLEDs for applications in displays and solid-lighting devices of various designs.[2] In terms of OLED structures, there are several important factors, such as the constituents of the host-dopant emitting layer of the energy transfer system,[3,4] the introduction of multilayer structures for effective carrier injection and transport,[5] the pretreatment or proper selection of the anode materials to ensure a good interface between the electrode and organic layers,[6,7] and the insertion of transition metal oxides such as MoO_3,[8] V_2O_5,[9] NiO,[10] and WO_3[11] between the electrode and organic layer to increase the carrier injection and transport through the improvement of interface performance by control of their work functions.

New transparent conducting oxides (TCOs) have attracted attention as alternative anode materials to indium tin oxide (ITO), and are thus another key issue in the development of OLED devices. Currently, ITO is the most commonly used TCO electrode for OLED devices because of its high electrical conductivity, transmittance, and high work function. However, ITO has many drawbacks, including its chemical instability, its potential for harm to human health, and its high cost due to the relative scarcity of indium (In).[12,13] Furthermore, In ions can lead to degradation of OLEDs by diffusion into the organic materials.[14] For these reasons, there is a great deal of research investigating alternatives to ITO.

In particular, among the alternative TCO materials, zinc oxide (ZnO), which is typically an n-type wide band gap semiconductor, is regarded as a representative TCO material and has excellent features such as high chemical stability, low material cost, high conductivity, and high optical transmittance. Moreover, the conductivity, optical transmittance, and work

Received: January 12, 2013
Accepted: March 28, 2013
Published: March 28, 2013

 © 2013 American Chemical Society

Table 1. Sample Identification (I.D.), Work Function (eV), and OLED Device Characteristics

sample I.D.	work function (eV)	turn-on voltage at 10 cd/m^2 (V)	turn-on voltage at 100 cd/m^2 (V)	turn-on voltage at 1000 cd/m^2 (V)	max. luminance at voltage (cd/m^2 at 20 V)	max. current efficiency (cd/A)
AZO_{Ref}	4.21	4.4	5.6	7.6	15400	7.7
AZO_{Buff}(3.1)	4.45	4.1	5.1	7.2	16890	12.1
AZO_{Buff}(4.1)	4.64	3.9	4.9	6.7	20290	13.4
AZO_{Buff}(5.1)	4.70	4.1	5.1	7.5	17270	13.1

function of ZnO can be controlled by impurity doping with various trivalent metals as electron donors into the ZnO matrix.[15,16] Al-doped ZnO (AZO) films are considered to be a suitable TCO electrode material for OLEDs due to their cost effectiveness, stability, nontoxic nature, and the abundance of Al; moreover, they are easily fabricated using various deposition methods. The fabrication of AZO films deposited by sputtering and PLD methods has been demonstrated for use in TCO electrodes in optoelectronic devices, including OLEDs,[12,16,17] photovoltaic cells,[18] and thin film transistors.[19] In particular, Xu et al.[12] reported OLED device performance with an AZO anode deposited by a sputtering method, which showed a low resistivity and high transmittance of 4×10^{-4} Ω cm and over 90%, respectively. However, the sputtering method for the deposition of TCO anodes has some drawbacks such as physical damage to the film surface and the lack of in situ control of the impurity doping concentration. Therefore, in the field of OLED application of AZO films, atomic layer deposition (ALD) technique was previously used to fabricate the AZO anode for In-free OLED as reported by Meyer et al.[20] On the other words, as a novel deposition technique, ALD is considered suitable for thin film deposition, as it is a cost-effective and low-temperature chemical deposition process. ALD employs atomic-scale deposition by controlling the film growth to under several angstroms (Å) per cycle.[21] Accordingly, the electrical, optical, and structural properties of thin films deposited by ALD can be easily and exactly modified and controlled by deposition conditions such as quantity of impurities, the doping concentration, and the deposition temperature.[22−25]

In this work, we studied ALD-AZO films for application in OLED devices in order to ascertain their performance as TCO anodes. These films contained a homogeneous buffer layer to improve the interface properties between the TCO anode and the organic layer. In order to investigate the effects of the homogeneous buffer layer on the operating performance of OLED devices, 10-nm-thick AZO anode buffer layers with Al doping concentrations of 3.1, 4.1, and 5.1 at % Al were grown at a thickness of 10 nm onto a 140-nm-thick AZO anode film containing 2.1 at % Al to control the work function of the buffer layer on the anode. This concept of the introduction of a buffer layer between the anode and organic layer originated from the work function variation of AZO films as a function of Al doping concentration. The AZO buffer layer, which has a higher work function than that of the AZO anode, is expected to play the role of a transition metal oxide such as MoO_3, V_2O_5, NiO, and WO_3, in order to improve the OLED device performance through effective hole injection and transport from the AZO anode to the organic layer. Moreover, in this investigation, the AZO buffer layer can be formed simultaneously on the AZO anode using an ALD process. Furthermore, the performance of OLED devices with an AZO anode and an incorporated homogeneous AZO buffer layer were investigated to determine the variation in the work function with the Al doping concentration in the buffer layers. Finally, their luminance and current efficiency characteristics were investigated through a comparison with control devices prepared with or without a homogeneous AZO buffer layer.

EXPERIMENTAL SECTION

Preparation of an AZO Anode with a Homogeneous AZO Buffer Layer. The prepared AZO films were grown using a flow-type ALD reactor (Lucida D100, NCD Co., Ltd., Korea) on Corning 1737 glass substrates with dimensions of 2.5 cm × 2.5 cm at a deposition temperature of 200 °C under a base pressure of 50 mTorr. The total AZO film thickness in combination with the AZO anode and AZO buffer layer was fixed at 150 nm. A 150-nm-thick AZO anode without a buffer layer as a reference film was prepared by deposition of 29 total "super cycles" with 2.1 at % Al. AZO anodes composed of ZnO and AlO_x were formed using a "super cycle" process, which was composed of sequential steps of 15 ZnO cycles, 1 AlO_x cycle, and 15 ZnO cycles where the surface of the film was terminated by ZnO rather than AlO_x. The growth rates per cycle (GPC) of ZnO and AlO_x were calculated from the prepared film thicknesses to be 1.70 Å/cycle and 1.10 Å/cycle at a deposition temperature of 200 °C, respectively. Diethyl zinc ($(C_2H_5)_2Zn$, DEZ) and deionized water (H_2O) were used as the precursor reactants for ZnO, while trimethyl aluminum ($Al(CH_3)_3$, TMA) and H_2O were used for AlO_x. High purity nitrogen (99.999% N_2) gas was used as the purge gas. The pulse times for each DEZ, TMA, and H_2O cycle were 0.1, 0.05, and 0.1 s, respectively, and the N_2 purge time was 10 s.

The 10-nm-thick AZO buffer layers consisted of different Al doping concentrations of 3.1, 4.1, and 5.1 at % Al. Growth of the AZO buffer layers was performed successively after the formation of ALD-AZO anodes at 200 °C. The deposition conditions of each AZO buffer layer were as follows: an AZO buffer layer of 3.1 at % Al deposited using three super cycles of ZnO:AlO_x:ZnO at 10:1:10 cycle ratios, an AZO buffer layer of 4.1 at % Al deposited using four super cycles of ZnO:AlO_x:ZnO at 8:1:7 cycle ratios, and an AZO buffer layer of 5.1 at % Al deposited using five super cycles of ZnO:AlO_x:ZnO at 6:1:6 cycle ratios. The 150-nm-thick AZO anode without a buffer layer was used as a reference sample, and the 140-nm-thick AZO anodes with 10-nm-thick buffer layers containing 3.1 at % Al, 4.1 at % Al, and 5.1 at % Al are denoted by AZO_{Ref}, AZO_{Buff}(3.1), AZO_{Buff}(4.1), and AZO_{Buff}(5.1), respectively (Table 1).

Fabrication of OLED Devices onto AZO Anodes with AZO Buffer Layers. To apply the OLED devices as a TCO anode and buffer layer, the AZO_{Ref}, AZO_{Buff}(3.1), AZO_{Buff}(4.1), and AZO_{Buff}(5.1) films were cleaned using acetone, methanol, deionized water (DI water; H_2O), and isopropyl alcohol in an ultrasonic bath. The films were then patterned by conventional photolithography and etched over the 2 mm × 2 mm emitting area by a wet process using a mixed etchant solution of MA-SO_2 (HCl:HNO_3 based acid solution, Dongwoo Fine-Chem. Cop.):H_2O = 1:10 for 20 s. The OLED devices with a structure of N1,N1′-(biphenyl-4,4′-diyl)bis(N1-phenyl-N4,N4-dimtolylbenzene-1,4-diamine) [DNTPD, 50 nm]/1,1-bis[(di-4-tolylamino) phenyl] cyclohexane [TAPC, 30 nm]/bis(10-hydroxybenzo [h]quinolinato) beryllium [$Bebq_2$, 30 nm]:10% doped RP-411/4,7-diphenyl-1,10-phenanthroline [Bphen, 50 nm]/LiF [1 nm]/Al [150 nm] were fabricated onto the AZO_{Ref}, AZO_{Buff}(3.1), AZO_{Buff}(4.1), and AZO_{Buff}(5.1) films. All organic and cathode materials were deposited by thermal evaporation under a pressure of 5×10^{-7} Torr.

dx.doi.org/10.1021/am400140c | ACS Appl. Mater. Interfaces 2013, 5, 3650−3655

DNTPD was used as a hole injection layer (HIL) and effectively reduced the lowest unoccupied molecular orbital (LUMO) energy barrier between the anode and the TAPC hole transport layer (HTL). TAPC acted as a hole transport into the emission layer as well as an electron blocking layer (EBL) with an energy gap 1.0 eV higher than the highest occupied molecular orbital (HOMO). The electron emission layer (EML) was composed of $Bebq_2$ as a host and RP-411 as a red phosphorescent dopant. Bphen was used as an electron transport layer (ETL) and a hole blocking layer (HBL), while LiF/Al was used as the electron injection layer (EIL) and cathode. Figure 1 shows the

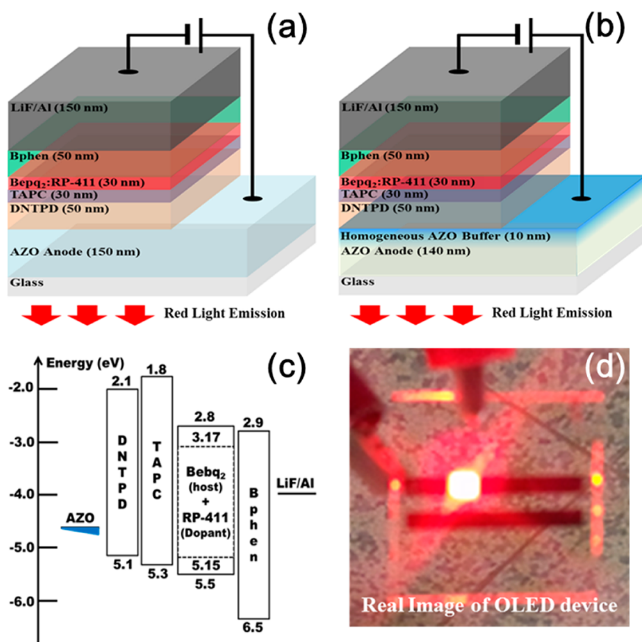

Figure 1. Device architecture of the OLED devices fabricated on (a) an AZO anode without a buffer layer (control device), (b) an AZO anode with an AZO homogeneous buffer layer, (c) the corresponding energy band diagram of the device, and (d) the real image of the OLED device on an AZO anode with an homogeneous AZO buffer layer (AZO_{Buff}(4.1)).

OLED device structure fabricated on (a) a 150-nm-thick AZO anode (AZO_{Ref} film) as a control device and (b) a 140-nm-thick AZO anode with a 10-nm-thick AZO buffer layer (AZO_{Buff}(3.1), AZO_{Buff}(4.1), and AZO_{Buff}(5.1) films). Panels c and d in Figure 1 show a schematic of the energy band diagram of the OLED device and real image of the OLED device on an AZO anode with an homogeneous AZO buffer layer (AZO_{Buff}(4.1)).

Characterization of AZO Anode Films and OLED Devices. The crystal structure and surface morphology of the AZO anode films were analyzed by X-ray diffraction (XRD, D/MAX-2000, Rigaku) with $CuK\alpha_1$ radiation and field emission scanning electron microscopy (FE-SEM, S-4800, Hitachi). A quantitative analysis of Al doping concentration was conducted using energy dispersive spectroscopy (EDS). The electrical resistivity of the AZO films was measured using a Hall-effect measurement system (HMS-3000, Ecopia) under 10 mA and a 0.57 T electromagnetic field. The transmittance of the AZO films was inspected using a UV−vis−NIR spectrometer (V-570, Jasco). Ultraviolet photoelectron spectroscopic (UPS) analysis was performed with He I (21.22 eV) radiation and a bias voltage (−5 V) in the 4D beamline of the Pohang Accelerator Laboratory (PLS). Au foil was used as a reference material for the calibration of the kinetic energy shift. The electrical and optical characteristics of the OLED as a function of the AZO anodes were investigated using an $I-L-V$ measurement system (M6100, McScience) in a dark room.

RESULTS AND DISCUSSION

Optical, Electrical, And Structural Properties of AZO Anode Films with Homogeneous AZO Buffer Layers. Figure 2 shows the optical transmittance curves of AZO anode

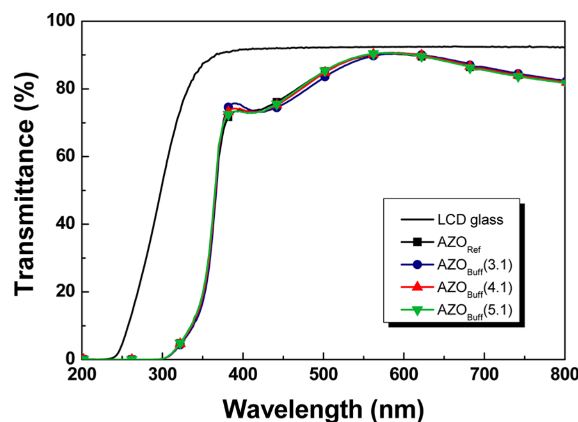

Figure 2. Optical transmittance spectra of AZO films with and without AZO buffer layers deposited on glass substrates in the range from 200 to 800 nm.

films without and with AZO buffer layers of 3.1, 4.1, and 5.1 at % Al. As shown, the optical transmittance curves of the AZO anode films showed a similar shape with or without an AZO buffer layer. The average transmittance values of the films were about 85% in the visible region from 400 to 800 nm and were about 90% at a wavelength of 550 nm, which is the maximum sensitivity of the human eye. The optical properties of the AZO anode film did not significantly change with the insertion of an AZO buffer layer due to the very low thickness and the small difference in the doping concentration from the AZO_{Ref} film.

Figure 3 shows the carrier concentration, the mobility, and the resistivity of AZO anode films with and without AZO buffer

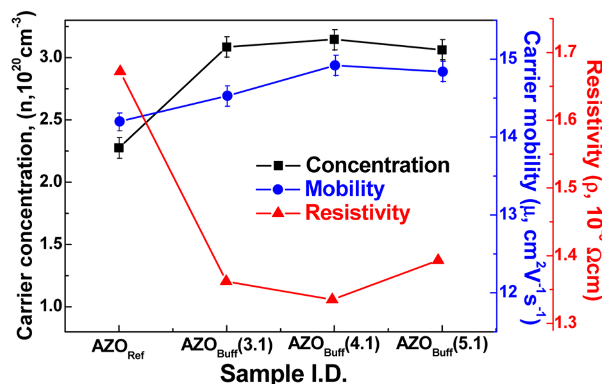

Figure 3. Hall parameters of AZO films without and with AZO buffer layers deposited on glass substrates.

layers. The films showed n-type semiconductor characteristics. The carrier concentration and the mobility values of the AZO_{Ref} film were 2.3×10^{20} cm^{-3} and 14.2 cm^2 V^{-1} s^{-1}, and increased up to 3.2×10^{20} cm^{-3} and 14.9 cm^2 V^{-1} s^{-1} with the AZO_{Buff}(4.1) film. The lowest resistivity value of 1.34×10^{-3} Ω cm was obtained with AZO_{Buff}(4.1), and the value was slightly increased with increasing Al doping concentration to 5.1 at %. Banerjee et al.[23] showed that a metastable $(ZnO)_3(Al_2O_3)$ phase could be formed during the formation of AZO films by

ALD and Lu et al.[26] reported that the metastable Al_2O_3 phase would be found in AZO films fabricated by DC magnetron sputtering. These metastable $ZnAl_2O_4$ and Al_2O_3 phases in AZO films have been known to decrease the conductivity of AZO films because they act as carrier trap sites and scattering centers.

To ascertain the crystalline variation in the AZO anode films as a function of the insertion of the AZO buffer layer, we performed phase analysis and morphological studies using XRD and FE-SEM, respectively. Figure 4 shows the XRD spectra of

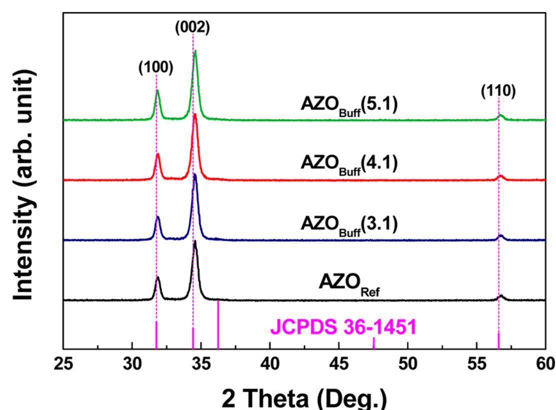

Figure 4. XRD diffraction patterns of AZO films without and with AZO buffer layers deposited on glass substrates.

the AZO anode films. The main diffraction peaks of the AZO_{Ref} film at 2θ angles of 31.88, 35.54, and 56.72° were indexed as 100, 002, and 110, respectively, with a hexagonal wurzite structure of ZnO.[22] The peak positions were slightly shifted to higher angles when compared with undoped ZnO (JCPDS 36–1451), as shown in Figure 4. A contraction of the unit cell could be clearly observed in all films based on the difference in the ionic radii of Zn^{2+} (~0.74 Å) and Al^{3+} (~0.54 Å).

Figure 5 shows the surface morphologies of the AZO anode films, which were obtained using FE-SEM. The surface morphology of the AZO_{Ref} film corresponds to a wedgelike shape. However, the $AZO_{Buff}(5.1)$ film showed a surface morphology different from that of the AZO_{Ref} film due to the formation of spinel $ZnAl_2O_4$ or metastable $(ZnO)_3(Al_2O_3)$ phases originating from high Al doping, which induces a decrease in the electrical conductivity of the AZO film.

Work Function Variation of AZO Anode Films with Homogeneous AZO Buffer Layers. UPS spectra for the secondary cutoff region and valence band spectra region were collected using a He I ($h\nu$ = 21.22 eV) energy source, and the results are shown in Figure 6a. The spectrum was taken with a

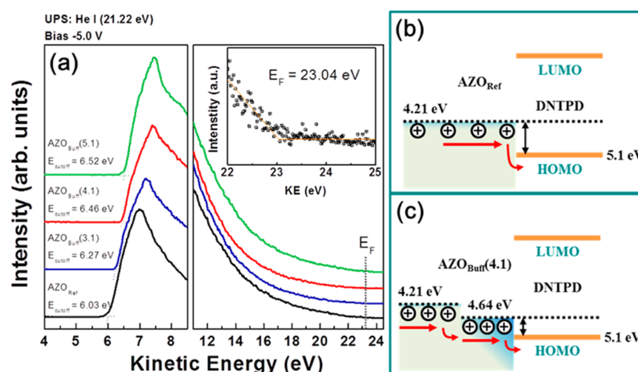

Figure 6. UPS spectra of (a) the low kinetic energy cutoff region and the valence band region of AZO films with and without AZO buffer layers, and (b, c) the corresponding energy diagrams at the anode/hole injection layer (HIL) interface.

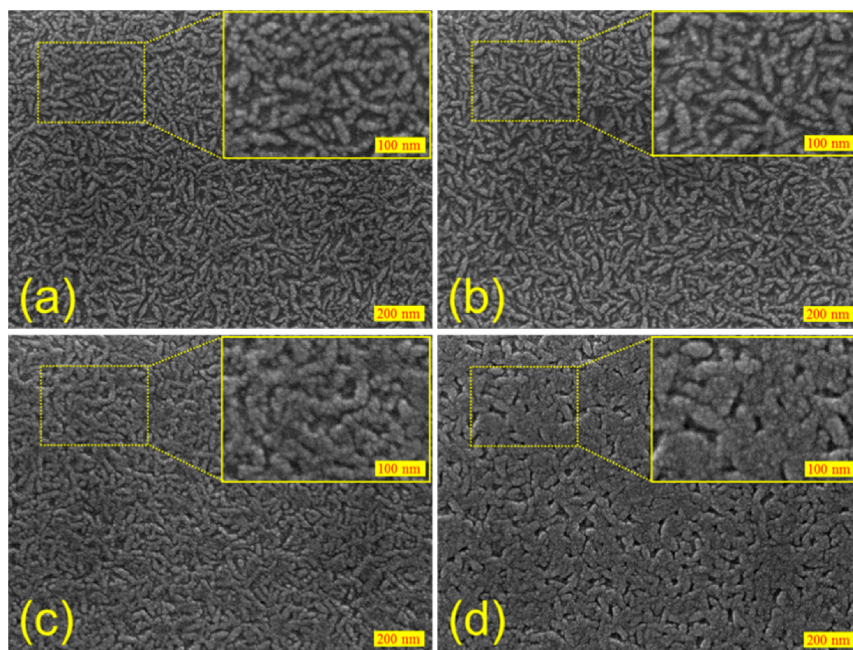

Figure 5. Top view FE-SEM images of (a) an AZO film without an AZO buffer layer (AZO_{Ref}) and AZO films with AZO buffer layers containing (b) 3.1 at % Al ($AZO_{Buff}(3.1)$), (c) 4.1 at % Al ($AZO_{Buff}(4.1)$), and (d) 5.1 at % Al ($AZO_{Buff}(5.1)$). Enlarged images are of the region indicated by a dotted box.

dx.doi.org/10.1021/am400140c | ACS Appl. Mater. Interfaces 2013, 5, 3650–3655

−5.0 V sample bias so that the sample inelastic cutoff could be distinguished from that due to the spectrometer. The Fermi energy (E_F) of the films was 23.04 eV, as indicated by the onset of energy intensity in the inset of Figure 6a. The work function of the films was determined using eq 1[27]

$$\Phi = h\upsilon + E_{cutoff} - E_F \quad (1)$$

From eq 1, the work functions of AZO_{Ref}, $AZO_{Buff}(3.1)$, $AZO_{Buff}(4.1)$, and $AZO_{Buff}(5.1)$ films were 4.21, 4.45, 4.64, and 4.70 eV, respectively, which is summarized in Table 1. The work function values of the AZO films clearly increased with an increase in Al doping concentration in the 10-nm-thick buffer layer.[17] An increase in the Al content in the buffer layer might induce a formation of nonconducting AlO_x layers,[28,29] which are resulted by the highly existence of metastable phases on the surface region and a variation of work function of the films. This result suggests that the work function of the AZO anode surface in the OLED device can be controlled by the insertion of a homogeneous AZO buffer layer regulating the Al doping concentration. Therefore, it is possible that an improvement in OLED performance can be achieved by a simple and continuous ALD process by correlating OLED device performance with the work function of the TCO anode since an increase in the work function makes the injection of holes from the organic layer to the anode easier (Figure 6b, c).

Characteristics of OLED Devices Fabricated onto AZO Anode Films with a Homogeneous AZO Buffer Layer. The characteristics of OLED devices fabricated on the AZO anode with and without an anode buffer layer are summarized in Table 1. Figure 7 shows the current density versus voltage

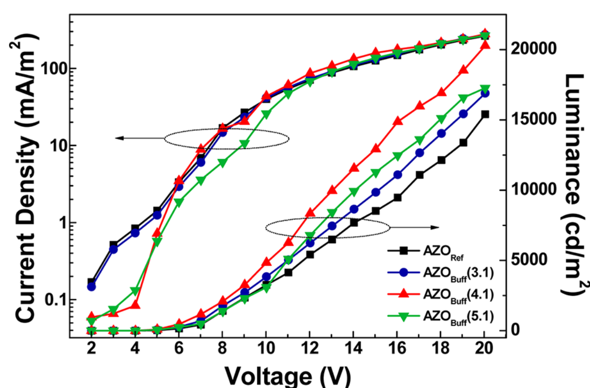

Figure 7. Current density versus luminance versus voltage ($J-L-V$) characteristics of the OLED devices fabricated onto AZO anodes with and without AZO buffer layers.

($J-V$) and the luminance versus voltage ($L-V$) characteristics of OLED devices employing an AZO anode with homogeneous AZO buffer layers as a function of Al doping concentration. The current density values at 20 V of OLED devices fabricated onto AZO anodes with an AZO buffer layer were slightly increased by introducing the AZO buffer layer. The current densities at 20 V were 262.8, 274.4, 278.8, and 267.5 mA/cm^2 for AZO_{Ref}, $AZO_{Buff}(3.1)$, $AZO_{Buff}(4.1)$, and $AZO_{Buff}(5.1)$, respectively. The luminance values of all prepared OLED devices with incorporated AZO buffer layers were improved relative to that of an AZO anode without an AZO buffer layer. The maximum luminance values of OLED devices were 15400, 16890, 20290, and 17270 cd/m^2 for AZO_{Ref}, $AZO_{Buff}(3.1)$, $AZO_{Buff}(4.1)$, and $AZO_{Buff}(5.1)$, respectively, at a bias of 20 V. Moreover, the turn-on voltage was considerably reduced through the introduction of an AZO buffer layer. Further, the turn-on voltage gap of OLED devices without and with an AZO buffer layer becomes more important at higher luminance values. At a luminance of 10 cd/m^2, the turn-on voltage values of OLED devices were 4.4, 4.1, 3.9, and 4.1 V for AZO_{Ref}, $AZO_{Buff}(3.1)$, $AZO_{Buff}(4.1)$, and $AZO_{Buff}(5.1)$, respectively. At a luminance of 1000 cd/m^2, the turn-on voltage values were 7.6, 7.2, 6.7, and 7.5 V, respectively. These results were due to a decrease in the electrical resistivity of the AZO anode with an AZO buffer layer, and an increase in the work function of the AZO anode with the buffer layer. The energy barrier at the interface between the AZO anode and DNTPD HIL was 0.89 eV, and this was reduced due to the introduction of an AZO buffer layer by 0.65, 0.46, and 0.40 eV for $AZO_{Buff}(3.1)$, $AZO_{Buff}(4.1)$, and $AZO_{Buff}(5.1)$, respectively. Consequently, hole injection and transport were improved due to a reduced energy barrier at the interface, in which hole transport could occur from the AZO anode to the DNTPD HIL more effectively. Therefore, the optimum OLED device performance (including current density, luminance, and turn-on voltage) was obtained with the OLED device fabricated on $AZO_{Buff}(4.1)$ in this work. This is because the $AZO_{Buff}(4.1)$ has the lowest resistivity value as well as a high enough work function value to lower the hole injection barrier between the AZO anode and DNTPD HIL. On the other hand, the performance of the OLED device with the $AZO_{Buff}(5.1)$ film was degraded due to a dramatic increase in resistivity; however, this device still showed higher performance due to effective hole injection by the highest work function in comparison to the performance of the OLED device without AZO buffer layer.

Similar to the result shown in Figure 7, higher current efficiency OLED devices were obtained for devices that included an AZO buffer layer when compared to the control sample, as shown in Figure 8. The maximum current density of

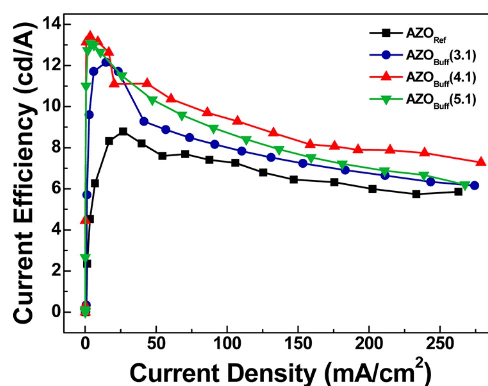

Figure 8. Current efficiency versus current density (E_c-J) characteristics of the OLED devices fabricated onto AZO anodes with and without AZO buffer layers.

an OLED device fabricated onto an AZO anode without a buffer layer was 8.8 cd/A, and that of $AZO_{Buff}(3.1)$, $AZO_{Buff}(4.1)$, and $AZO_{Buff}(5.1)$ were improved, with values of 12.1, 13.4, and 13.0 cd/A, respectively. In particular, the current efficiency increased remarkably in the low current density region (under 20 mA/cm^2) because a high luminance value was obtained at a low turn-on voltage, and then current efficiency decreased linearly. On the basis of these results, the AZO buffer layer significantly influences the performance of

OLED devices through decreasing resistivity and increasing the work function.

■ CONCLUSION

In this work, we studied the effect of the adoption of a homogeneous AZO buffer layer with different AZO anode compositions deposited using ALD on the performance of OLED devices. The AZO buffer layer does not influence the transmittance or crystallinity of the AZO anode film. But, the resistivity of the AZO anode film was decreased for concentrations up to 4.1 at % Al in the AZO buffer layer (AZO_{Buff}(4.1)). The resistivity of the AZO film incorporated with AZO_{Buff}(5.1) increased because the high Al−doping concentration induced the formation of $ZnAl_2O_4$ or $(ZnO)_3(Al_2O_3)$ phases. The work function of the AZO anode films continuously increased with increases in the Al doping concentration in the AZO buffer layer. Therefore, the OLED device performance in terms of luminance, current efficiency, and turn-on voltage was improved by introducing an AZO buffer layer since the effectiveness of hole injection and transport between the AZO anode and DNTPD HIL was increased. Therefore, the insertion of a homogeneous AZO buffer layer into an AZO anode can improve the characteristics of OLED devices by controlling the nature of the interface in terms of resistivity and work function, and this coherent combination of an anode and a homogeneous buffer layer can also be applied to any kind of OLED structure.

■ AUTHOR INFORMATION

Corresponding Author

*E-mail: hhpark@yonsei.ac.kr. Tel: 82-2-2123-2853. Fax: 82-2-312-5375.

Author Contributions

‡Authors Y.-J.C. and S.C.G. contributed equally to this work.

Notes

The authors declare no competing financial interest.

■ ACKNOWLEDGMENTS

This research was supported by the Basic Science Research Program through the National Research Foundation of Korea (NRF) funded by the Ministry of Education, Science and Technology (2012R1A6A3A01015896). Further support was provided by the Industrial Strategic Technology Development Program (10041926, development of high density plasma technologies for thin film deposition of nanoscale semiconductor and flexible display processing) funded by the Ministry of Knowledge Economy (MKE, Korea). Experiments at PLS were supported in part by MEST and POSTECH.

■ REFERENCES

(1) Logothetidis, S. *Mater. Sci. Eng., B* **2008**, *152*, 96−104.
(2) D'Andrade, B. W.; Forrest, S. R. *Adv. Mater.* **2004**, *16*, 1585−1595.
(3) Pereira, A.; Gallardo, H.; Conte, G.; Quirino, W. G.; Legnani, C.; Cremona, M.; Bechtold, I. H. *Org. Electron.* **2012**, *13*, 90−97.
(4) Lee, Y. H.; Ju, B.-K.; Jeon, W. S.; Kwon, J. H.; Park, O. O.; Yu, J.-W.; Chin, B. D. *Synth. Met.* **2009**, *159*, 325−330.
(5) Kulkarni, A. P.; Tonzola, C. J.; Babel, A.; Jenekhe, S. A. *Chem. Mater.* **2004**, *16*, 4556−4573.
(6) Park, Y. W.; Jang, J. H.; Kim, Y. M.; Choi, J. H.; Park, T. H.; Choi, J.; Ju, B. K. *Thin Solid Films* **2009**, *517*, 4108−4110.
(7) Li, C. N.; Kwong, C. Y.; Djurišić, A. B.; Lai, P. T.; Chui, P. C.; Chan, W. K.; Liu, S. Y. *Thin Solid Films* **2005**, *477*, 57−62.
(8) Wang, F.; Qiao, X.; Xiong, T.; Ma, D. *Org. Electron.* **2008**, *9*, 985−993.
(9) Wu, J.; Hou, J.; Cheng, Y.; Xie, Z.; Wang, L. *Semicond. Sci. Technol.* **2007**, *22*, 824−826.
(10) Im, H. C.; Choo, D. C.; Kim, T. W.; Kim, J. H.; Seo, J. H.; Kim, Y. K. *Thin Solid Films* **2007**, *515*, 5099−5102.
(11) Meyer, J.; Winkler, T.; Hamwi, S.; Schmale, S.; Johannes, H.-H.; Weimann, T.; Hinze, P.; Kowlasky, W.; Riedl, T. *Adv. Mater.* **2008**, *20*, 3839−3843.
(12) Xu, D.; Deng, Z.; Xu, Y.; Xiao, J.; Liang, C.; Pei, Z.; Sun, C. *Phys. Lett. A* **2005**, *346*, 148−152.
(13) Chen, T. L.; Ghosh, D. S.; Krautz, D.; Cheylan, S.; Pruneri, V. *Appl. Phys. Lett.* **2011**, *99*, 093302.
(14) So, F.; Kondakov, D. *Adv. Mater.* **2010**, *22*, 3762−3777.
(15) Kelly, P. J.; Zhou, Y. *J. Vac. Sci. Technol. A* **2006**, *24*, 1782−1789.
(16) Kim, H.; Horwitz, J. S.; Kim, W. H.; Mäkinen, A. J.; Kafafi, Z. H.; Chrisey, D. B. *Thin Solid Films* **2002**, *420−421*, 539−543.
(17) Jiang, X.; Wong, F. L.; Fung, M. K.; Lee, S. T. *Appl. Phys. Lett.* **2003**, *83*, 1875−1877.
(18) Schulze, K.; Maennig, B.; Leo, K.; Tomita, Y.; May, C.; Hüpkes, J.; Brier, E.; Reinold, E.; Bäuerle, P. *Appl. Phys. Lett.* **2007**, *91*, 073521.
(19) Yun, D.-J.; Rhee, S.-W. *Thin Solid Films* **2009**, *517*, 4644−4649.
(20) Meyer, J.; Görrn, P.; Hamwi, S.; Johannes, H.-H.; Riedl, T.; Kowalsky, W. *Appl. Phys. Lett.* **2008**, *93*, 073308.
(21) George, S. M. *Chem. Rev.* **2010**, *110*, 111−131.
(22) Dasgupta, N. P.; Neubert, S.; Lee, W.; Trejo, O.; Lee, J. R.; Prinz, F. B. *Chem. Mater.* **2010**, *22*, 4769−4775.
(23) Banerjee, P.; Lee, W.-J.; Bae, K.-R.; Lee, S. B.; Rubloff, G. W. *J. Appl. Phys.* **2010**, *108*, 043504.
(24) Pung, S.-Y.; Choy, K.-L.; Hou, X.; Shan, C. *Nanotechnology* **2008**, *19*, 435609.
(25) Elam, J. W.; George, S. M. *Chem. Mater.* **2003**, *15*, 1020−1028.
(26) Lu, J. G.; Ye, Z. Z.; Zeng, Y. J.; Zhu, L. P.; Wang, L.; Yuan, J.; Zhao, B. H.; Liang, Q. L. *J. Appl. Phys.* **2006**, *100*, 073714.
(27) Yun, D.-J.; Hong, K.; Kim, S. H.; Yun, W.-M.; Jang, J.-Y.; Kwon, W.-S.; Park, C. E.; Rhee, S.-W. *ACS Appl. Mater. Interfaces* **2011**, *3*, 43−49.
(28) Kim, W.-H.; Maeng, W. J.; Kim, M.-K.; Kim, H. *J. Electrochem. Soc.* **2011**, *158*, D495−D499.
(29) Kim, T. W.; Choo, D. C.; No, Y. S.; Choi, W. K.; Choi, E. H. *Appl. Surf. Sci.* **2006**, *253*, 1917−1920.